Applied Surface Science 520 (2020) 146298

Contents lists available at ScienceDirect

Applied Surface Science

journal homepage: www.elsevier.com/locate/apsusc

Engineering black titanium dioxide by femtosecond laser filament

Yue Su[a], Wei Zhang[a], Shanming Chen[a], Danwen Yao[a], Jilian Xu[b], Xiaobo Chen[c,*], Lei Liu[b,*], Huailiang Xu[a,d,e,*]

[a] State Key Laboratory on Integrated Optoelectronics, College of Electronic Science and Engineering, Jilin University, Changchun 130012, China
[b] State Key Laboratory of Luminescence and Applications, Changchun Institute of Optics, Fine Mechanics and Physics, CAS, Changchun 130033, China
[c] Department of Chemistry, University of Missouri-Kansas City, MO 64110, USA
[d] State Key Laboratory of Precision Spectroscopy & Chongqing Institute, East China Normal University, Shanghai 200062, China
[e] CAS Center for Excellence in Ultra-intense Laser Science, Shanghai 201800, China

ARTICLE INFO

Keywords:
Titanium dioxide
Femtosecond laser filamentation
Absorption enhancement
Disordered surface
Laser processing
Solar energy

ABSTRACT

We propose an approach, by utilizing the propagation of femtosecond laser pulses in the filamentation region in air, to achieve black titanium dioxide (TiO_2), a promising material for efficient photocatalysis. It is found that the black TiO_2 engineered by femtosecond laser filament in both solution and air environments shows significantly improved absorption in a broad spectral range from 400 to 2500 nm. In addition, the engineered black TiO_2 shows a certain degree of enhanced absorption in the microwave range. The structural and elemental analyses of the processed TiO_2 suggest that the absorption enhancement is mainly ascribed to the filament-induced disorder and dopant impurity in the surface layer of crystalline TiO_2. Our technique provides an alternative way to engineer black TiO_2 with the capability of absorbing the solar energy across a broad spectrum that can be useful for various applications in optoelectronics and photochemistry.

1. Introduction

Titanium dioxide (TiO_2), a promising photocatalyst for sustainable environment applications, has been extensively studied, e.g., for solar hydrogen generation [1,2], water splitting [3–5], and environmental pollutant removal [6]. The efficiency of TiO_2 for harvesting solar energy, however, is limited by its energy bandgap of more than 3.0 eV [7], which only allows TiO_2 to absorb sunlight in the ultraviolet (UV) region that accounts for about 5% of the available solar energy on Earth [8]. A variety of approaches have thus been developed for extending the TiO_2 absorption from UV to visible and IR spectral ranges that cover most of energy of natural sunlight radiation. For example, it was demonstrated that the optical properties of TiO_2 can be effectively modified by introducing the electron and hole traps in the band gap with metal and non-metal elements doping [9–11], by forming a composite materials with narrowband semiconductors or molecules [12,13], by engineering the lattice structures through hydrogenation [14,15], as well as by forming Ti^{3+} species and surface disorder using a high energy nanosecond laser ablation of TiO_2-suspended solution [16,17].

On the other hand, among various material processing techniques, femtosecond laser pulses that possess the unique features of high-peak power and ultrashort duration have been shown to enable modifications of optical, mechanical as well as wetting properties of a variety of soft and hard materials such as polymer, semiconductor, glass and crystal [18–21]. However, the reports on the modification of optical properties of TiO_2 by femtosecond laser processing are very rare till now. The difficulty may result from the involvement of tight focusing in near-field femtosecond laser processing that makes it time consuming and not easily applicable to nano-sized particles as well as irregularly shaped surfaces.

Recently, it was demonstrated that a femtosecond laser filament-based far-field technique can remotely and rapidly fabricate nano/microstructures on crystalline silicon as well as on irregularly shaped organic and metals surfaces for improved light absorption [22–26]. This technique is based on the unique nonlinear phenomenon resulting from the propagation of powerful laser pulses in transparent media, which can confine the light in a thin channel called filament [27]. The typical diameter of a filament in air is ~100 μm with a length far beyond the Rayleigh range of the input laser beam which ranges from a few centimeters to meters, depending on the external focusing and input laser energy. The laser intensity inside the filament core is clamped at the range of 10^{13}–10^{14} W/cm^2 in air.

In the present study, we investigate the feasibility of modifying the absorption properties of TiO_2 by irradiating TiO_2 nanoparticles with

* Corresponding authors.
E-mail addresses: chenxiaobo@umkc.edu (X. Chen), liulei@ciomp.ac.cn (L. Liu), huailiang@jlu.edu.cn (H. Xu).

https://doi.org/10.1016/j.apsusc.2020.146298
Received 11 February 2020; Received in revised form 11 March 2020; Accepted 7 April 2020
Available online 13 April 2020
0169-4332/

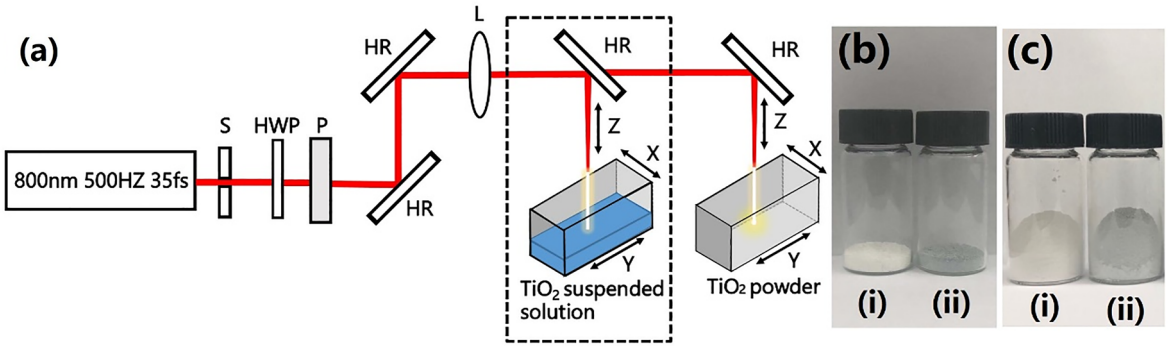

Fig. 1. (a) Schematic diagram of the experimental setup for femtosecond laser filament processing of TiO_2 suspended in water as well as TiO_2 powder in air. S: shutter; HWP: half wave plate; P: polarizer; L: fused silica lens; HR: 800-nm high reflective lens. (b) The unprocessed TiO_2 (i) and the processed samples obtained by irradiating the filament on the interfere of TiO_2 suspended solution with air (ii). (c) The unprocessed TiO_2 (i) and the processed samples obtained by irradiating the filament on the surface of dye TiO_2 powder in air (ii).

femtosecond laser filament in both an ambient air and a solution environment. We demonstrate that the absorption properties of micro-sized TiO_2 particles can be efficiently modified over a broad spectral range from visible to infrared, and even microwave range. After performing the reflection, Raman, energy dispersive spectroscopy (EDS) and X-ray diffraction (XRD) spectroscopic analyses of the engineered black TiO_2, we find that the improved optical absorption of the black TiO_2 particles may result mainly from filament-induced disorder and nitrogen dopant in the surface layer.

2. Experimental setup

The schematic diagram of the experimental setup was shown in Fig. 1(a). A commercial Ti: Sapphire laser system (Spectra-Physics, Spitfire ACE) was used to produce linearly polarized femtosecond laser pulses with a central wavelength of 800 nm, a repetition rate of 500 Hz, and a pulse width of 35 fs. An electrical shutter enables simple and fast control of the pulse train. A rotatable half wave plate and a polarizer were inserted in the laser propagation path to control the laser pulse energy. Before the pulses passing through the focusing lens, the height of the beam was adjusted by using two 800-nm high reflective lens to facilitate vertical downward scanning of the sample.

The powder sample of anatase TiO_2 with the size of 70–100 nm was first placed in a rectangular container and flattened with a glass slide to facilitate filament ablation. The rectangular container with TiO_2 was mounted on a platform equipped on a two-dimensional motorized stage, which enabled rapid scanning of the sample by continuously moving the stage in a raster way. The flattened surface of the TiO_2 powder samples was perpendicular to the laser beam propagation direction, and placed in the middle position of the filament to ensure the interaction of the TiO_2 powder with the laser pulses inside the filament. The scanning speed was set at 10 mm/s and the distance between adjacent scanning lines was set at 100 μm. As shown in Fig. 1a, we performed the experiments in two environments: one is to irradiate the filament generated with a 25-cm focal lens and 1.8-mJ laser energy on the surface of TiO_2 suspended water solution (see the dashed square area), and the other is to irradiate the filament generated with a 1-m focal lens and 1-mJ laser energy on the surface of dye TiO_2 powder in air. As a result, Fig. 1(b, c) shows the photos of the untreated titanium dioxide and the processed samples under the two experimental conditions. It can be seen for both cases that the color of the samples turns from the original white to the grayish black after the filament ablation.

The optical properties of the processed samples from the visible to the near-infrared region were characterized by using a spectrophotometer (UV-3600, Shimadzu Company) equipped with an integrating sphere (LISR-UV). The complex permittivity and permeability were measured at the frequency range of 1–18 GHz using a HP8722ES network analyzer. In order to analyze the crystal structures of the processed TiO_2, the XRD patterns of the processed samples were obtained by a Rigaku D/MAX 2550 diffractometer. A Raman spectrometer (model LabRAM HR Evolution by Horriba Scientific) with a 532 nm laser as the excitation source was used to examine the structural change on the surface of the processed samples. The elemental composition analysis was performed using an energy dispersive spectrometer (EDS, EDAX AMETEK).

3. Results and discussions

To understand the color changes of the processed TiO_2 samples shown in Fig. 1(b) and (c), we first investigate the morphologies of the TiO_2 samples before and after the filament treatment. Fig. 2 shows the SEM images of (a) the pristine and (b, c) the processed TiO_2 in the solution (b) and air (c) conditions with a 10 mm/s scanning speed. It can be seen from Fig. 2 that the SEM images do not reveal significant differences in the morphologies of the pristine TiO_2 and the processed TiO_2 by the filament in solution and air conditions. The averaged sizes of the unprocessed and processed TiO_2 particles are almost the same with a typical diameter of 70–90 nm, indicating that the high-intensity

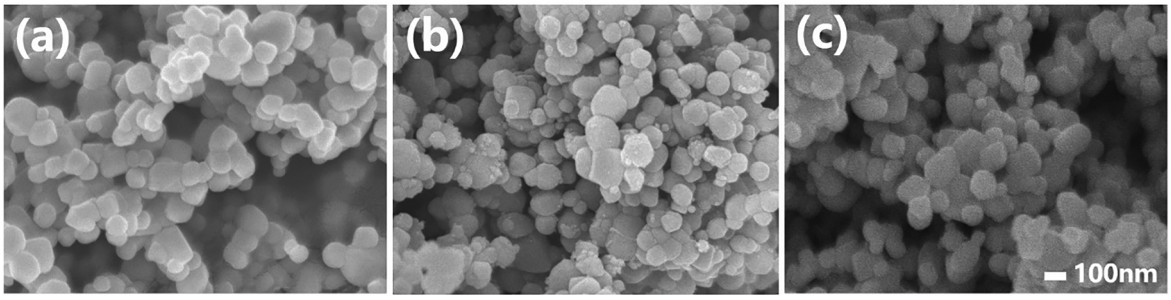

Fig. 2. SEM images of (a) the pristine TiO_2 and (b, c) the filament-processed TiO_2 particles in the (b) solution and (c) air conditions.

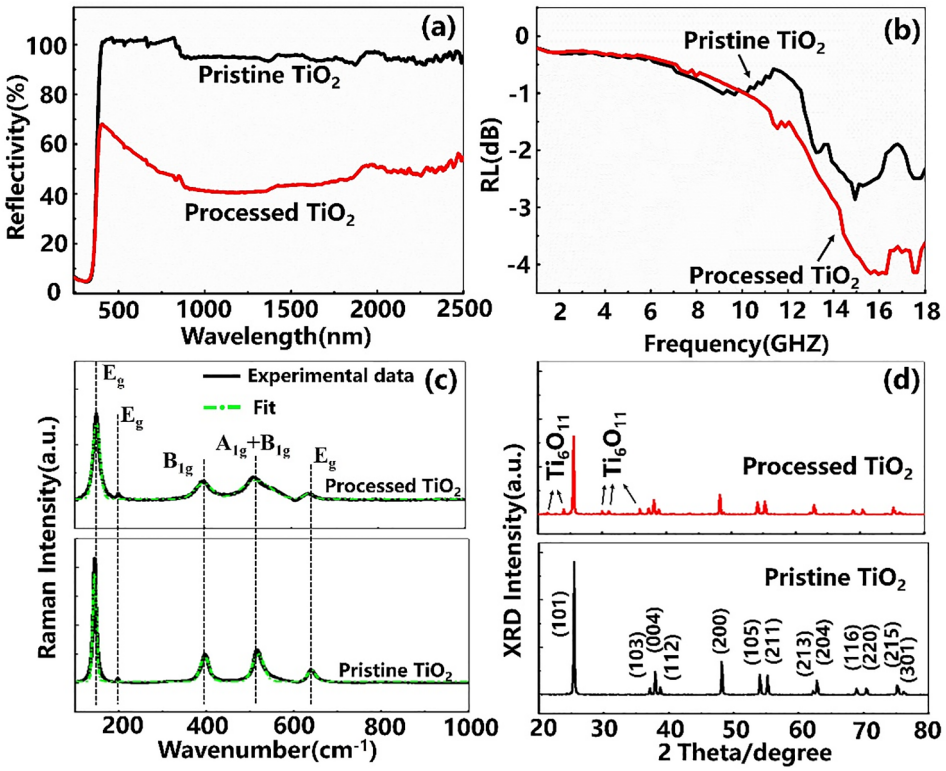

Fig. 3. UV–visible-NIR reflection (a), GHz RL (b), Raman (c) and XRD (d) spectra of the unprocessed TiO_2 and the processed samples in the solution condition.

femtosecond filament processing does not induce significant change in the geometrical structure of TiO_2 nanoparticles. This may result from the fact that the initial gas peak temperature inside the air filament is about 1000 K [28], which is much lower than the melting point of TiO_2 (~2100 K [29]). This result is different from those TiO_2 nanoparticles processed with high-energy nanosecond laser pulses, in which the sizes of TiO_2 nanoparticles vary significantly due to the much higher nanosecond laser ablation temperature [17]. In addition, from the SEM images we cannot observe any nano structured patterns on the TiO_2 particles. Therefore, it is evident from the SEM images that the color change of the processed TiO_2 samples is not due to the morphologies of TiO_2 samples.

We then investigated the optical property and crystalline structure of TiO_2 nanoparticles by measuring reflection, Raman, XRD spectra of the unprocessed and processed TiO_2 nanoparticles in the solution environment. In Fig. 3(a), the UV–visible-NIR reflection spectra of the unprocessed TiO_2 and the processed samples are shown, from which it can be seen that the pristine TiO_2 has an almost 100% reflectivity in the visible and near-infrared spectral range, and only absorbs ultraviolet light with wavelengths below 400 nm. After the filament processing, the reflectivity decreases by about 40–50% over the broad range of 400–2500 nm, indicating that the absorption of the processed TiO_2 nanoparticles is extended from ultraviolet up to near-infrared spectral region. Clearly, the filament processing effectively enhances the absorption of TiO_2 in the visible and near-infrared light region, giving rise to the color change in Fig. 1(b). With more efficient light absorption in such a broad spectral range, it makes these nanoparticles valuable in many applications, such as photoelectric detectors [30–32], photovoltaic devices [33,34], and photocatalyst reactions [2,14].

Furthermore, we examined the absorption property of the pristine TiO_2 and the filament-processed TiO_2 nanoparticles in the microwave range. The microwave absorption of TiO_2 was evaluated with the complex permittivity ε_r ($=\varepsilon'$-$j\varepsilon''$) and permeability values μ_r ($=\mu'$-$j\mu''$), where the real parts ε' and μ' are the electric and magnetic field energy stored in the medium, and the imaginary part ε'' and μ'' are the dissipated electric and magnetic field energy. By measuring the frequency profiles of the dielectric (ε' and ε'') and magnetic (μ' and μ'') constants of the pristine and processed TiO_2 samples in the microwave region of 1–18 GHz, the microwave reflection loss (RL) curve can be calculated according to the following equations [35]

$$RL(dB) = 20\lg |(Z_{in} - Z_0)/(Z_{in} + Z_0)|, \quad (1)$$

$$Z_{in} = Z_0\sqrt{\mu_r/\varepsilon_r}\, tahh\left[j\left(\frac{2\pi fd}{c}\right)\sqrt{\frac{\mu_r}{\varepsilon_r}}\right], \quad (2)$$

where f, d, c, Z_0, Z_{in} and RL(dB) are the frequency of the electromagnetic wave, the thickness of the absorber, the velocity of light, the impedance of the free space, the input impedance of the absorber, and RL(dB) the reflection loss in dB, respectively. As a result, the calculated RL values are shown in Fig. 3(b), from which it can be seen that the filament-processed TiO_2 can absorb microwaves more efficiently than the pristine TiO_2 in the range of 10–18 GHz, and the extreme RL values can approximately reach −4.0 dB. Therefore, the above results clearly indicate that the TiO_2 samples have a certain degree of absorption enhancement in the microwave region induced by the filament processing.

To reveal the mechanism behind the improved absorption of the engineered TiO_2 by filament. We measured the Raman spectra of the unprocessed and processed TiO_2 nanoparticles, as shown in Fig. 3(c). For anatase TiO_2, the six Raman active modes are usually observed, namely Ti−O bond stretching vibration modes E_g(639 cm^{-1}), B_{1g} (519 cm^{-1}), and A_{1g} (515 cm^{-1}) and O−Ti−O bending-type vibration modes B_{1g}(399 cm^{-1}), E_g (197 cm^{-1}), and E_g (144 cm^{-1}) [36]. As can be shown in Fig. 3(c), the pristine white TiO_2 displays strong and sharp typical anatase Raman bands, while for the processed black TiO_2 samples the anatase peaks become broader. By fitting the experimental data (solid line) to a Gaussian function (dash line), we determined the full width at half-maximum (FWHM) of the Raman modes, and found that for the processed sample, the FWHMs of the Raman modes at 143 cm^{-1}, 396 cm^{-1}, 517 cm^{-1}, and 639 cm^{-1} are respectively

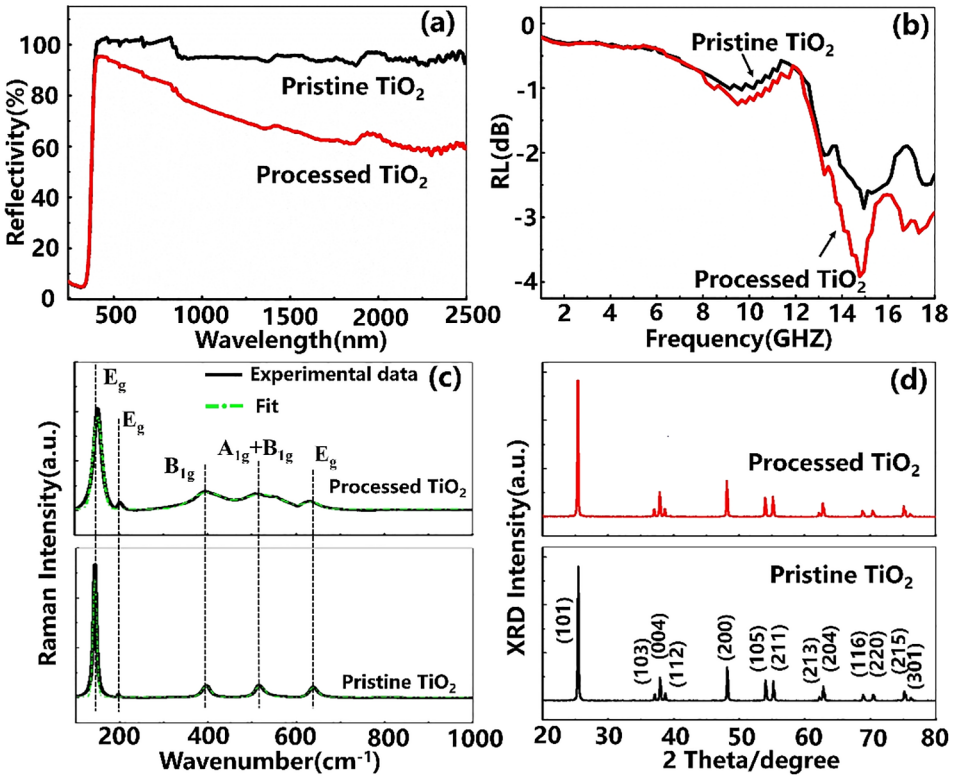

Fig. 4. UV–visible-NIR reflection (a), GHz RL (b), Raman (c) and XRD (d) spectra of the unprocessed TiO_2 and the processed samples in the air condition.

increased by about 85%, 93%, 159% and 17%, which indicates that the filament processing may change the surface layer of the TiO_2 structure from crystalline to amorphous.

We also conducted the crystal structures analysis of the unprocessed TiO_2 and the processed samples with XRD spectra, as shown in Fig. 3(d). For the sample before the filament processing, the sample exhibits the typical anatase XRD features, and the strong diffraction peaks can be identified as the (1 0 1), (1 0 3), (0 0 4), (1 1 2), (2 0 0), (1 0 5), (2 1 1), (2 1 3), (2 0 4), (1 1 6), (2 2 0), (2 1 5) and (3 0 1) lattice planes of anatase. While for the filament-processed sample, several new diffraction peaks located at 21.5°, 24.0°, 29.9°, 31.0°, and 35.8° appear, which can be assigned to Ti_6O_{11}, indicating that reduction reactions may occur resulting in the appearance of low-priced titanium ions. Since the XRD can penetrate the samples, the new appeared XRD peaks under the solution condition may show that part of the crystalline TiO_2 in the inner core changes from crystalline to amorphous.

In the air condition, the optical properties of the processed TiO_2 samples were also characterized. Fig. 4(a) and (b) show the UV–visible-NIR reflectance spectra and the GHz reflection loss values of the unprocessed and the processed TiO_2 samples, respectively. As shown in Fig. 4(a), the reflectivity of the processed samples gradually decreases as the wavelength increases, which becomes less than 60% at the wavelength of 2500 nm. In addition, according to the calculated RL values shown in Fig. 4(b), the filament-ablated TiO_2 samples have a certain degree of absorption enhancement in the microwave region, and the extreme RL values can approximately reach −4.0 dB at about 14 GHz. Clearly, the above results indicate that, similar to those shown in Fig. 3, the optical properties of processed samples can be efficiently modified by irradiating TiO_2 nanoparticles in air with femtosecond laser filament.

As a consequence, by processing TiO_2 nanoparticles by femtosecond laser filament in both solution and air environments, the optical properties of TiO_2 nanoparticles can be efficiently modified over a broad spectral range from visible to infrared, and even microwave range. However, when compared with those obtained in solution (Fig. 3), it can also be seen from Fig. 4 that the reflectivity of the processed TiO_2 in air gradually decreases from visible to IR, and the improved absorption range in the GHz range is also narrower than that in Fig. 3(b).

To understand the difference between the reflectivity of the processed TiO_2 in Fig. 3 and Fig. 4, we also measured their Raman and XRD spectra before and after the filament processing in air. Similar to that shown in Fig. 3(c), the Raman spectra of the samples, shown in Fig. 4(c), indicates that the Raman peaks become broader. By curve fitting, we find that the FWHMs of the processed samples are increased by about 130%, 244%, 301% and 68%, for the Raman modes at E_g (143 cm^{-1}), B_{1g} (395 cm^{-1}), A_{1g} + B_{1g} (517 cm^{-1}), and E_g (638 cm^{-1}), respectively. This reveals clearly that the lattice disorder happens to the surface of the samples. The more broadened Raman lines in the air condition than those in the solution condition may indicate that the filament-induced disorder effect is more significant in the air condition. However, it can be seen from Fig. 4(d) that the XRD spectrum of the processed TiO_2 samples in air shows almost the same diffraction feature as that shown in Fig. 3(d), that is, no observable extra diffraction peaks appear in the air condition. Such differences between the XRD spectra presented in Fig. 3(d) and Fig. 4(d) may indicate that in the solution environment water molecules activate the reduction reaction during the filament processing. Therefore, based on the above analysis on Raman and XRD, the filament-processed TiO_2 nanoparticles under the air condition may only induce the phase transition on the surface layer from crystalline to amorphous.

To further reveal the absorption enhancement of the filament-processed TiO_2 samples, we also examined the chemical compositions of the processed TiO_2 under the two processing conditions by measuring their EDS spectra. Fig. 5 shows the actual distribution of elements of (a) the pristine and (b, c) the processed TiO_2 in the solution (b) and air (c) conditions. It can be clearly seen from Fig. 5 that when compared with the unprocessed samples, the processed TiO_2 sample in both solution and air conditions introduced nitrogen and generated oxygen vacancy, as shown in Fig. 5(b-c). The appearance of nitrogen element and oxygen vacancy may cause the formation of the disordered surface layer and

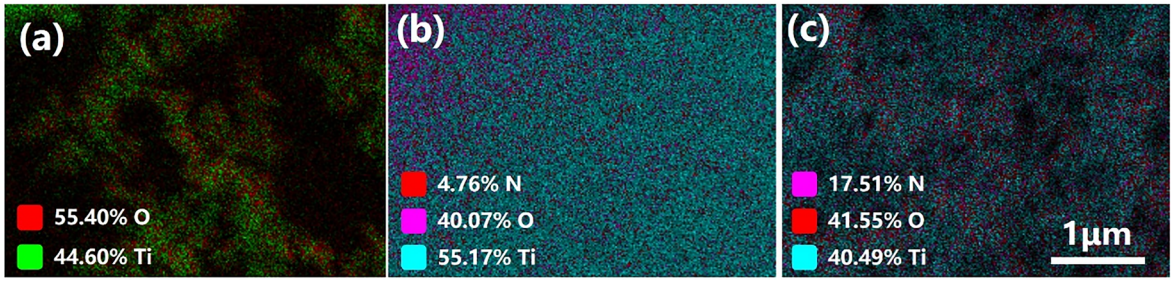

Fig. 5. The actual distribution of elements of (a) the pristine TiO_2 and (b, c) the filament-processed TiO_2 particles in the (b) solution and (c) air conditions.

the modification of the energy-band structure, resulting in an enhanced absorption for photon energy below the direct band gap in the visible and near-IR range shown in Figs. 3(a) and 4(a).

On the other hand, the improvement of microwave absorption may also be resulted from the generation of amorphous shell on the sample surface. Since the corresponding electronic structures and the dielectric constant of the amorphous-shell region are different from those of the crystalline TiO_2 inner core region, there exists charge accumulation between the phase boundaries, resulting in collective interface dipoles along the interfaces [6]. Furthermore, in comparison with the conventional hydrogenated black TiO_2 [6], it is found that the ε' value of the filament-processed TiO_2 sample is changed slightly. This in fact demonstrates the role of the disorder-disorder interface, which will greatly enhances the microwave absorption performance of TiO_2 nanoparticles.

4. Summary

In summary, we have demonstrated the feasibility of engineering black TiO_2 by irradiating anatase TiO_2 nanoparticles with femtosecond laser pulses in the filamentation regime. Under both the solution and air conditions, the engineered black TiO_2 shows significantly enhanced absorption in the visible and near-IR spectral range. Absorption enhancement in microwave range has also been observed. By analyzing structural and elemental information of the processed TiO_2 samples, we have found that the improvement in absorption is mainly attributed to the filament-induced disorder and dopant impurity in the surface layer. Our study suggests that femtosecond laser filament has the potential to engineer black TiO_2 for applications in optoelectronics and photochemistry.

CRediT authorstship contribution statement

Yue Su: Data curation, Validation, Formal analysis, Investigation, Resources and Writing-Original draft. **Wei Zhang:** Investigation, and Resources. **Shanming Chen:** Investigation, and Resources. **Danwen Yao:** Investigation, and Resources. **Jilian Xu:** Investigation, and Resources. **Xiaobo Chen:** Supervision, and Writing-Review and Editing. **Lei Liu:** Conceptualization, Methodology, Visualization, Funding acquisition, Suppervision, and Writing-Reviewing and Editing. **Huailiang Xu:** Conceptualization, Methodology, Investigation, Supervision, Visualization, Writing-Reviewing and Editing, Project administration, and Funding acquisition.

Declaration of Competing Interest

The authors declare that they have no known competing financial interests or personal relationships that could have appeared to influence the work reported in this paper.

Acknowledgement

The work is supported in part by National Natural Science Foundation of China (NSFC) (61625501, 61525404, 11704376), the Open Fund of the State Key Laboratory of High Field Laser Physics (SIOM), and the Program for JLU Science and Technology Innovative Research Team (JLUSTIRT) (2017TD-21), and Fundamental Research Funds for the Central Universities.

References

[1] Y. Ma, Q. Xu, R.F. Chong, C. Li, Photocatalytic H2 production on TiO_2 with tuned phase structure, J. Mater. Res. 28 (2013) 394–399.
[2] X.B. Chen, S.S. Mao, Titanium dioxide nanomaterials: synthesis, properties, modifications, and applications, Chem. Rev. 107 (2007) 2891–2959.
[3] X.D. Wang, J. Shi, Evolution of titanium dioxide one-dimensional nanostructures from surface-reaction-limited pulsed chemical vapor deposition, J. Mater. Res. 28 (2013) 270–279.
[4] J.B. Joo, Q. Zhang, M. Dahl, F. Zaera, Y.D. Yin, Synthesis, crystallinity control, and photocatalysis of nanostructured titanium dioxide shells, J. Mater. Res. 28 (2013) 362–368.
[5] X.B. Chen, C. Li, M. Grätzel, R. Kostecki, S.S. Mao, Nanomaterials for renewable energy production and storage, Chem. Soc. Rev. 41 (2012) 7909–7937.
[6] L.H. Tian, J.L. Xu, M. Just, M. Green, L. Liu, X.B. Chen, Broad range energy absorption enabled by hydrogenated TiO_2 nanosheets: from optical to infrared and microwave, J. Mater. Chem. C 5 (2017) 4645–4653.
[7] L. Liu, P.Y. Yu, X.B. Chen, S.S. Mao, D.Z. Shen, Hydrogenation and disorder in engineered black TiO_2, Phys. Rev. Lett. 111 (2013) 065505.
[8] T. Xia, C. Zhang, N.A. Oyler, X.B. Chen, Enhancing microwave absorption of TiO_2 nanocrystals via hydrogenation, J. Mater. Res. 29 (2014) 2198–2210.
[9] W. Choi, A. Termin, M.R. Hoffmann, Effects of metal-ion dopants on the photocatalytic reactivity of quantum-sized TiO_2 particles, Angew. Chem. Int. Ed. Engl. 33 (1994) 1091–1092.
[10] X.B. Chen, C. Burda, The electronic origin of the visible-light absorption properties of C-, N- and S-doped TiO_2 nanomaterials, J. Am. Chem. Soc. 130 (2008) 5018–5019.
[11] X.B. Chen, C. Burda, Photoelectron spectroscopic investigation of nitrogen-doped titania nanoparticles, J. Phys. Chem. B 108 (2004) 15446–15449.
[12] M. Dahl, Y.D. Liu, Y.D. Yin, Composite titanium dioxide nanomaterials, Chem. Rev. 114 (2014) 9853–9889.
[13] Y. Ma, X.L. Wang, Y.S. Jia, X.B. Chen, H.X. Han, C. Li, Titanium dioxide-based nanomaterials for photocatalytic fuel generations, Chem. Rev. 114 (2014) 9987–10043.
[14] X.B. Chen, L. Liu, P.Y. Yu, S.S. Mao, Increasing solar absorption for photocatalysis with black hydrogenated titanium dioxide nanocrystals, Science 331 (2011) 746–750.
[15] T. Xia, C. Zhang, N.A. Oyler, X.B. Chen, Hydrogenated TiO_2 nanocrystals: a novel microwave absorbing material, Adv. Mater. 25 (2013) 6905–6910.
[16] X. Chen, D.X. Zhao, K.W. Liu, C.R. Wang, L. Liu, B.H. Li, Z.Z. Zhang, D.Z. Shen, Laser modified black titanium oxide nanospheres and their photocatalytic activities under visible light, ACS Appl. Mater. Interfaces 7 (2015) 16070–16077.
[17] K.X. Li, J.L. Xu, X.D. Yan, L. Liu, X.B. Xiao, Y.S. Luo, J. He, D.Z. Shen, The origin of the strong microwave absorption in black TiO_2, Appl. Phys. Lett. 108 (2016) 183102.
[18] C.H. Crouch, J.E. Carey, M. Shen, E. Mazur, F.Y. Génin, Infrared absorption by sulfur-doped silicon formed by femtosecond laser irradiation, Appl. Phys. A: Mater. Sci. Process. 79 (2004) 1635–1641.
[19] C. Wu, C.H. Crouch, L. Zhao, J.E. Carey, R. Younkin, J.A. Levinson, E. Mazur, R.M. Farrell, P. Gothoskar, A. Karger, Near-unity below-band-gap absorption by microstructured silicon, Appl. Phys. Lett. 78 (2001) 1850–1852.
[20] P. Bizi-Bandoki, S. Benayoun, S. Valette, B. Beaugiraud, E. Audouard, Modifications of roughness and wettability properties of metals induced by femtosecond laser treatment, Appl. Surf. Sci. 7 (2011) 5213–5218.
[21] C.Z. Yao, Y.Y. Ye, B.S. Jia, Y. Li, R.J. Ding, Y. Jiang, Y.X. Wang, X.D. Yuan, Polarization and fluence effects in femtosecond laser induced micro/nano structures on stainless steel with antireflection property, Appl. Surf. Sci. 425 (2017)

1118–1124.
[22] X.P. Zhan, H.L. Xu, C.H. Li, H.W. Zang, C. Liu, J.H. Zhao, H.B. Sun, Remote and rapid micromachining of broadband low-reflectivity black silicon surfaces by femtosecond laser filaments, Opt. Lett. 42 (2017) 510–513.
[23] H.Y. Tao, J.Q. Lin, Z.Q. Hao, X. Gao, X.W. Song, C.K. Sun, Xin Tan, Formation of strong light-trapping nano- and microscale structures on a spherical metal surface by femtosecond laser filament, Appl. Phys. Lett. 100 (2012) 201111.
[24] Y. Su, X.P. Zhan, H.W. Zang, Y. Fu, A.W. Li, H.L. Xu, S.L. Chin, P. Polynkin, Direct and stand-off fabrication of black silicon with enhanced absorbance in the short-wavelength infrared region using femtosecond laser filament, Appl. Phys. B Lasers Opt. 124 (2018) 223.
[25] X.P. Zhan, Y.J. Wang, Y. Su, M.T. Li, H.W. Zang, H. Xia, H.L. Xu, B. Liu, H.B. Sun, Micro-Nano-texturing inner surfaces of small-caliber high-aspect-ratio and superhydrophobic artificial vessels using femtosecond laser filamenting pulses, Adv. Mat. Interfaces 5 (2018) 1801148.
[26] Y. Su, S.Q. Wang, D.W. Yao, Y. Fu, H.W. Zang, H.L. Xu, P. Polynkin, Stand-off fabrication of irregularly shaped, multi-functional hydrophobic and antireflective metal surfaces using femtosecond laser filaments in air, Appl. Surf. Sci. 494 (2019) 1007–1012.
[27] S.L. Chin, Femtosecond Laser Filamentation, Springer, New York, 2010.
[28] G. Point, C. Millián, A. Couairon, A. Mysyrowicz, A. Houard, Generation of long-lived underdense channels using femtosecond filamentation in air, J. Phys. B: At., Mol. Opt. Phys. 48 (2015) 094009.
[29] L. Lei, X.B. Chen, Titanium dioxide nanomaterials: Self-Structural modifications, Chem. Rev. 114 (2014) 9890–9918.
[30] F.G. Yan, Z.M. Wei, X. Wei, Q.S. Lv, W.K. Zhu, K.Y. Wang, Towards high performance photodetectors based on two dimensional materials: strategy on methods, Small Methods 2 (2018) 1700349.
[31] W.G. Luo, Y.F. Cao, P.A. Hu, K.M. Cai, Q. Feng, F.G. Yan, T.F. Yan, X.H. Zhang, K.Y. Wang, Gate tuning of high-performance InSe-based photodetectors using graphene electrodes, Adv. Opt. Mater. 3 (2015) 1418.
[32] X. Wei, F.G. Yan, Q.S. Lv, C. Shen, K.Y. Wang, Fast gate-tunable photodetection in the graphene sandwiched WSe2/GaSe heterojunctions, Nanoscale 9 (2017) 8388–8392.
[33] S.K. Kim, R.W. Day, J.F. Cahoon, T.J. Kempa, K.D. Song, H.G. Park, C.M. Lieber, Tuning light absorption in core/shell silicon nanowire photovoltaic devices through morphological design, Nano Lett. 12 (2012) 4971–4976.
[34] D. Duché, L. Escoubas, J.J. Simon, P. Torchio, W. Vervisch, F. Flory, Slow Bloch modes for enhancing the absorption of light in thin films for photovoltaic cells, Appl. Phys. Lett. 92 (2008) 193310.
[35] M. Green, Z. Liu, P. Xiang, X. Tian, F. Huang, L. Liu, X. Chen, Ferric metal-organic framework for microwave absorption, Mater. Today. Chem. 9 (2018) 140–148.
[36] T. Xia, N. Li, Y.L. Zhang, M.B. Kruger, J. Murowchick, A. Selloni, X.B. Chen, Directional heat dissipation across the interface in anatase-rutile nanocomposites, ACS Appl. Mater. Interfaces 5 (2013) 9883–9890.